

1 **Text S1. The calculation of nutrient flux**

2 In this study, the nutrients flux in North Pacific Ocean Desert (NPOD) is calculated to explain the
3 variation of NPOD seasonality, based on the ocean horizontal velocity components, temperature,
4 salinity data from SODA3 reanalysis data in 1998–2015. The nutrients field is assumed to be
5 consistent from 1998 to 2015 due to the lack of interannually-varying nutrients observations and
6 our focus on nutrients variations caused by ocean dynamical processes. A 1D K-profile
7 parameterization algorithm (Large et al., 1994) is driven by the ocean physics data to calculate
8 the vertical mixing coefficient (KM) in NPOD area. Therefore, nutrients flux to surface ocean
9 (across 10m depth) in 1998-2015 can be calculated by using the convective-diffusive equation
10 combined with the nutrients and KM data.

11 **Text S2. Description of data sources, Elman neural network and CMIP5 models.**

12 For observational and reanalysis data used in Sect. 3: Mapped Chl-a data from SeaWiFS and
13 MODIS-Aqua ocean color observation are available at NASA's OceanColor
14 (<https://oceandata.sci.gsfc.nasa.gov/directdataaccess/>). They are provided by NASA Goddard
15 Space Flight Center, Ocean Ecology Laboratory, Ocean Biology Processing Group (doi:
16 10.5067/ORBVIEW-2/SEAWIFS/L3M/CHL/2022, doi:
17 10.5067/AQUA/MODIS/L3M/CHL/2022). NOAA_OI_SST_V2 data and GODAS_SSH data are
18 provided by the NOAA/OAR/ESRL Physical Sciences Division, Boulder, Colorado, USA, from
19 their websites at <http://www.esrl.noaa.gov/psd/> and
20 <https://www.cpc.ncep.noaa.gov/products/GODAS/>. Solar radiation and precipitation data are
21 from ERA5 monthly averaged dataset generated by Copernicus Climate Change Service
22 (<https://cds.climate.copernicus.eu/cdsapp#!/dataset/reanalysis-era5-single-levels-monthly-means>,
23 doi: 10.24381/cds.f17050d7). Wind stress data are from ECMWF ORAS5 at [http://icdc.cen.uni-](http://icdc.cen.uni-hamburg.de/1/projekte/easy-init/easy-init-ocean.html?no_cache=1)
24 [hamburg.de/1/projekte/easy-init/easy-init-ocean.html?no_cache=1](http://icdc.cen.uni-hamburg.de/1/projekte/easy-init/easy-init-ocean.html?no_cache=1). Temperature, salinity, MLD
25 and current speed data from SODA3.3.1 are accessible at <http://www.atmos.umd.edu/~ocean/>.
26 Nutrients data can be found at WOA05
27 <https://www.nodc.noaa.gov/OC5/WOA05/pubwoa05.html>.

28 For the Elman neural network (ENN) in Sect. 4, the transfer functions are the hyperbolic
29 tangent sigmoid and Purelin for the hidden and the output layers, respectively. The maximum
30 epoch is set to 2000 and two hidden layers with 20 and 5 neurons are applied. For the ENN input,
31 we use modelling data from CMIP5 dataset which designs a set of future climate scenarios, called
32 Representative Concentration Pathways (RCP) scenarios. In RCP 8.5 experiment, Climate change

33 scenarios are forced by prescribed greenhouse gas and other natural forcings, and the radiative
34 forcing value is projected to rise to 8.5 W m^{-2} by 2100. The CMIP5 modelling outputs are at
35 monthly resolution from January 2006 to December 2100 and are averaged within NPOD region
36 and standardized (converted to Z-scores) before insertion into the ENN model.

37 We select five variables in the CMIP5 simulations include sea surface temperature (SST), sea
38 surface height, precipitation rate, wind curl and surface downwelling solar radiation, which is
39 highly linked with the interannual variation of NPOD: (a) SST can determine the thermal
40 stratification and change upward transport of nutrients. (b) sea surface height variation can
41 change the depth of nutricline and surface nutrient content (Thomas et al., 2012). (c) wind curl is
42 directly associated with the intensity of subtropical gyres, a dynamic process responsible for the
43 formation of NPOD. (d) atmospheric nutrients deposition changes the nutrients structure in the
44 surface ocean due to precipitation (Duce et al., 2008). (e) the decrease of surface solar radiation
45 contributes to the lowering in Chl-a concentration in 1998–2003 (Gregg et al., 2005). Based on
46 the sensitivity test of ENN performance to different input variables (Table S3), we select SST,
47 wind curl and solar radiation as the input data to the ENN. For the robustness of the future
48 projection, we also used the Chl-a output from seven models (see Fig.6) to calculate the NPOD-
49 area variation under the RCP 8.5 scenarios.

50

51

52

53

54

55

56

57

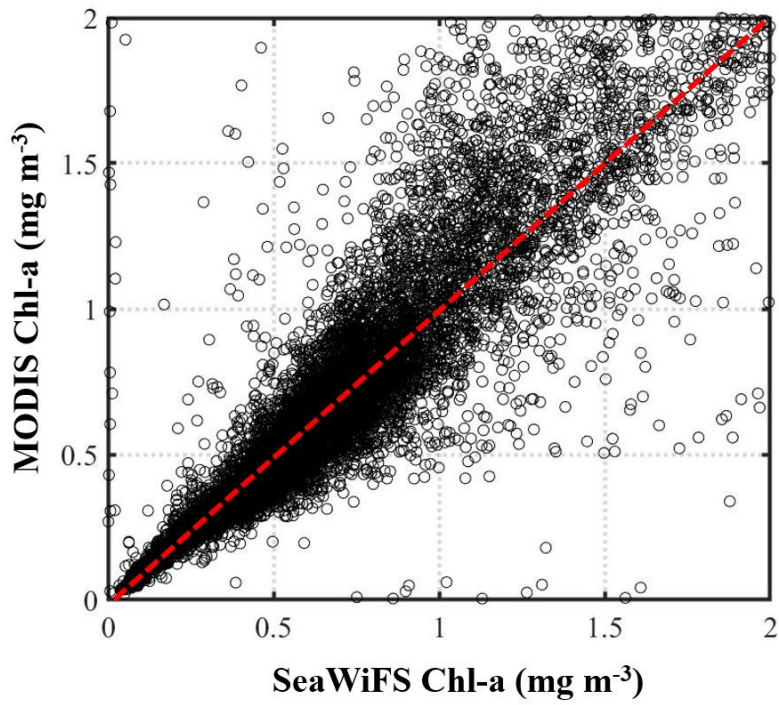
58

59

60

61

62



63

64 **Figure S1.** Comparison of monthly surface Chl-a concentration data in NPOD region during
65 2003–2007 retrieved by SeaWiFS and MODIS/Aqua.

66

67

68

69

70

71

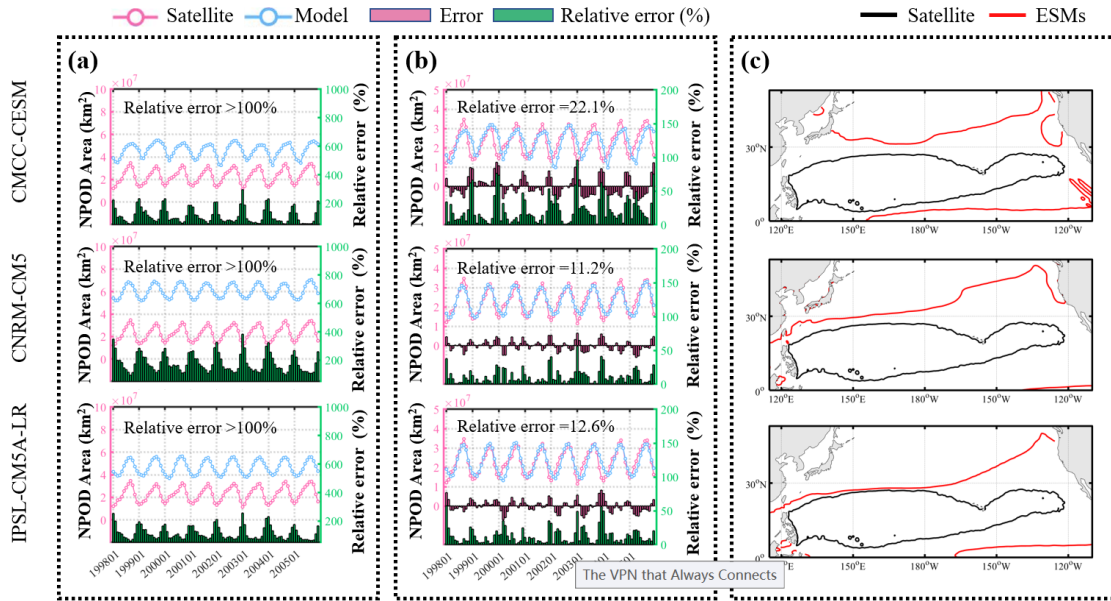
72

73

74

75

76



77

78 **Figure S2.** (a) Comparison of NPOD area calculated by satellite observations and simulated by
 79 three Earth System Models (ESMs), CMCC-CESM, CNRM-CM5, and IPSL-CM5A-LR in their
 80 hindcast simulations during 1998–2005. (b) Comparison of NPOD area seasonal cycles (by
 81 removing climatological mean NPOD area) calculated by satellite observations and simulated by
 82 ESMS. (c) Comparison of NPOD locations calculated by satellite observations and simulated by
 83 ESMS.

84

85

86

87

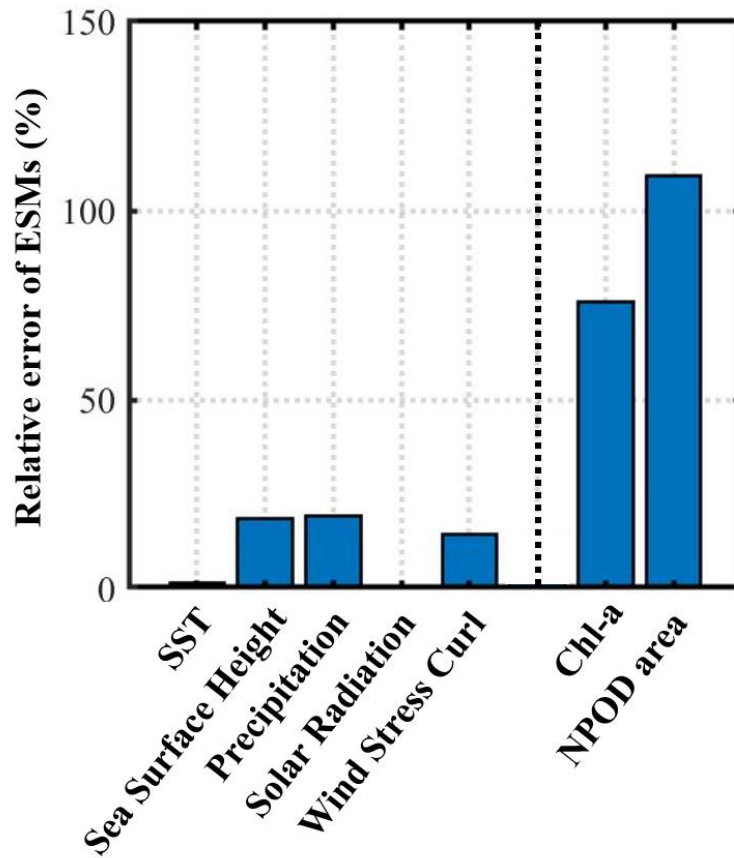
88

89

90

91

92



93

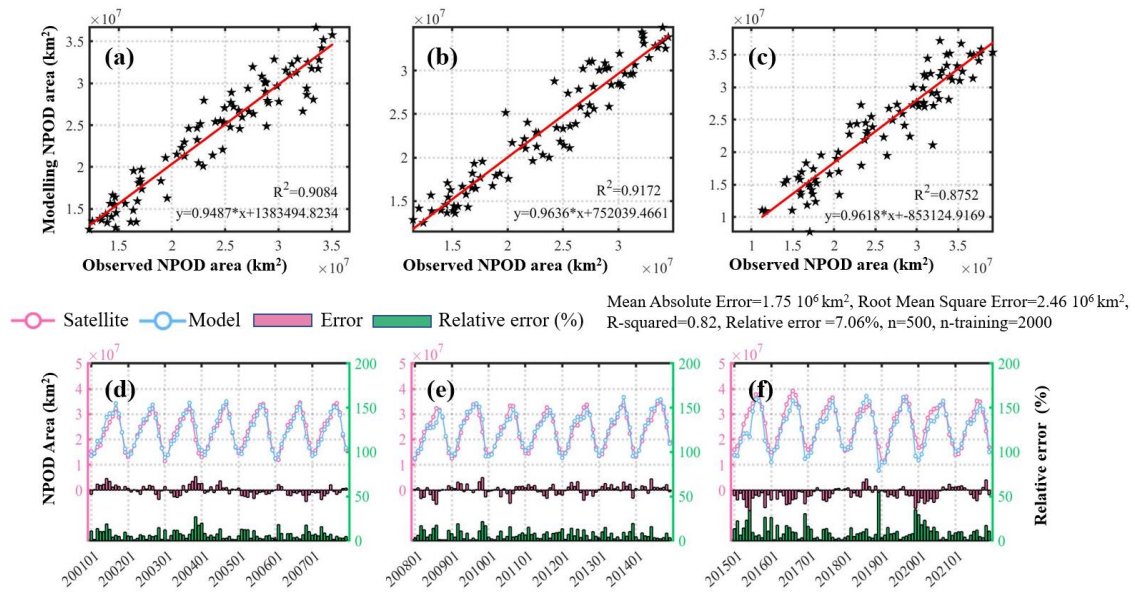
94 **Figure S3.** Relative error of multi-model average variables by CMCC-CESM, CNRM-CM5, and
 95 IPSL-CM5A-LR, relative to the observational and reanalysis data (see Text S2).

96

97

98

99



100

101 **Figure S4.** (a-c) Comparison of NPOD area calculated by satellite observations and predicted by
 102 ENN model in different phases. (d-f) Time series of NPOD area calculated by satellite
 103 observations (pink line) and simulated by ENN model (blue line), and the red and green bar
 104 charts represent the error and relative error of ENN prediction, respectively.

105

106

107

108

109

110

111

112

113

114

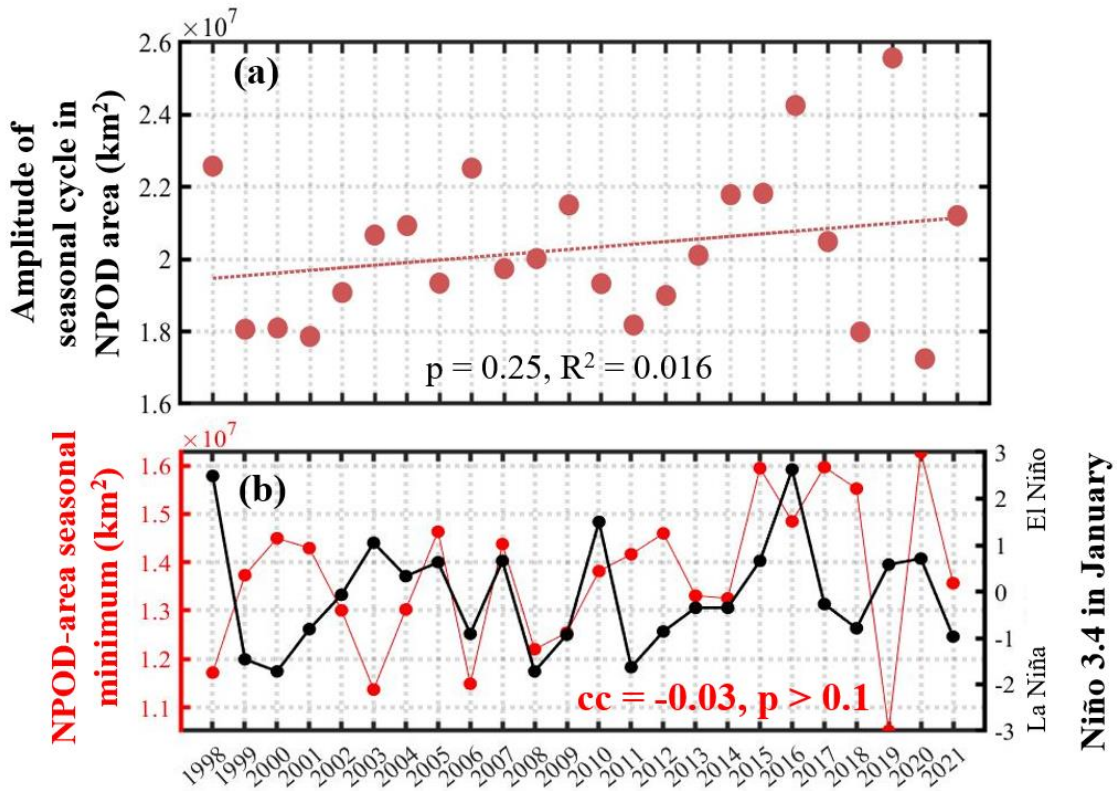
115

116

117

118

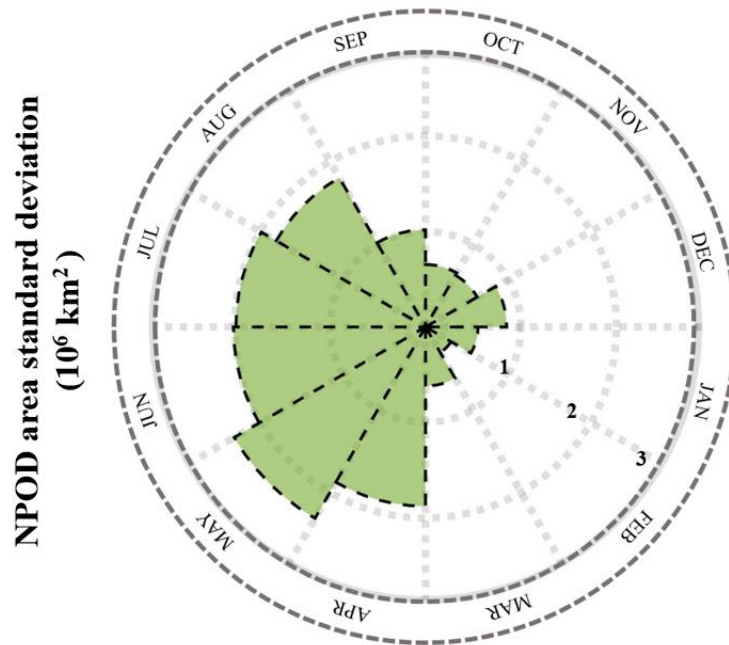
119



120

121 **Figure S5.** (a) Amplitude of the seasonal cycle in NPOD area in 1998–2021, red dashed line
 122 represents the linear-fitted trend. (b) Time series of NPOD area seasonal minimum (left axis) and
 123 Niño 3.4 index in January (right axis) in 1998–2021. "cc" represents the correlation coefficient.

124



125

126 **Figure S6.** Standard deviation of NPOD-area time series in 1998–2021 for specific month.

127

128

129

130

131

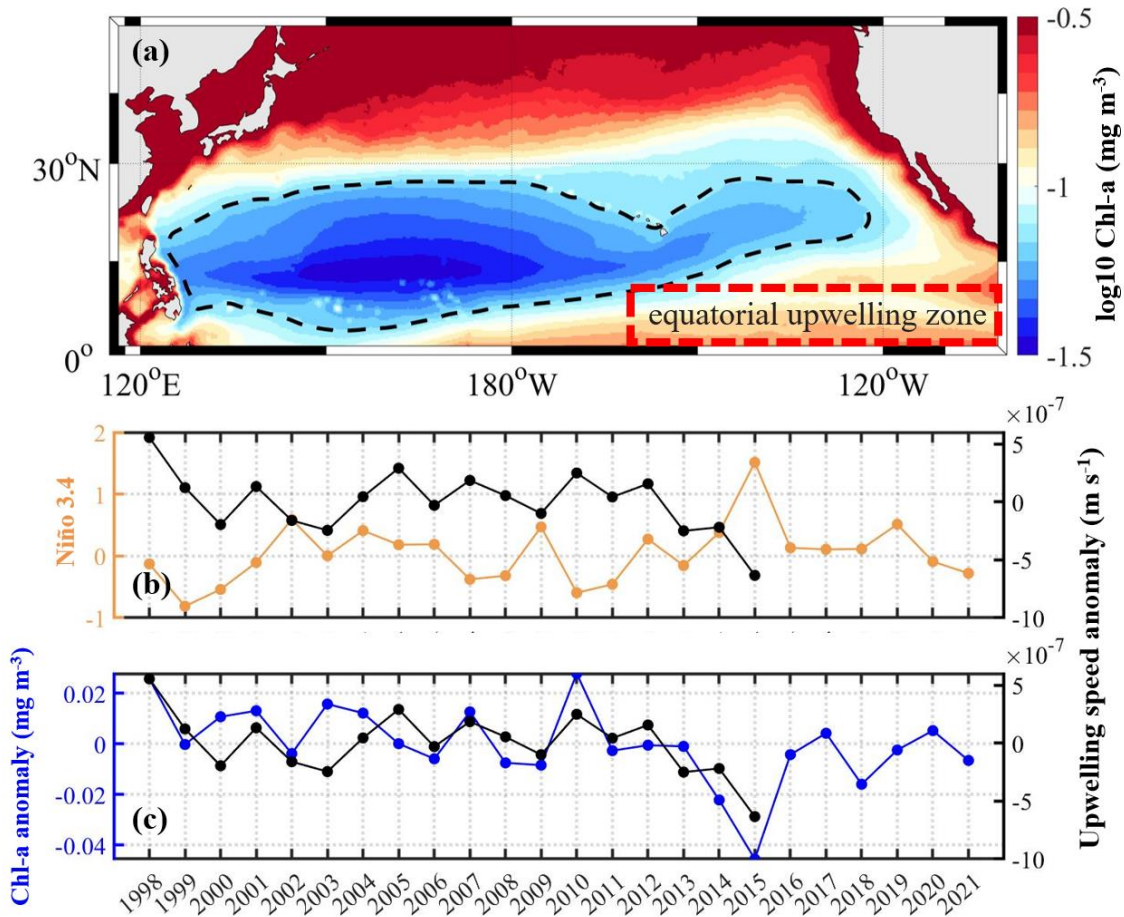
132

133

134

135

136



138

139 **Figure S7.** (a) Equatorial upwelling zone and NPOD geographical region (red box and black
 140 dashed line, respectively) with the color shadings representing ocean surface Chl-a concentration
 141 averaged during 1998–2021. (b) Time series of Niño 3.4 index (left axis) and upwelling speed
 142 anomaly (right axis) in equatorial upwelling zone in each summer half year (April–September) of
 143 1998–2021. (c) Time series of Chl-a concentration anomaly (left axis) and upwelling speed
 144 anomaly (right axis) in equatorial upwelling zone in each summer half year.

145

146

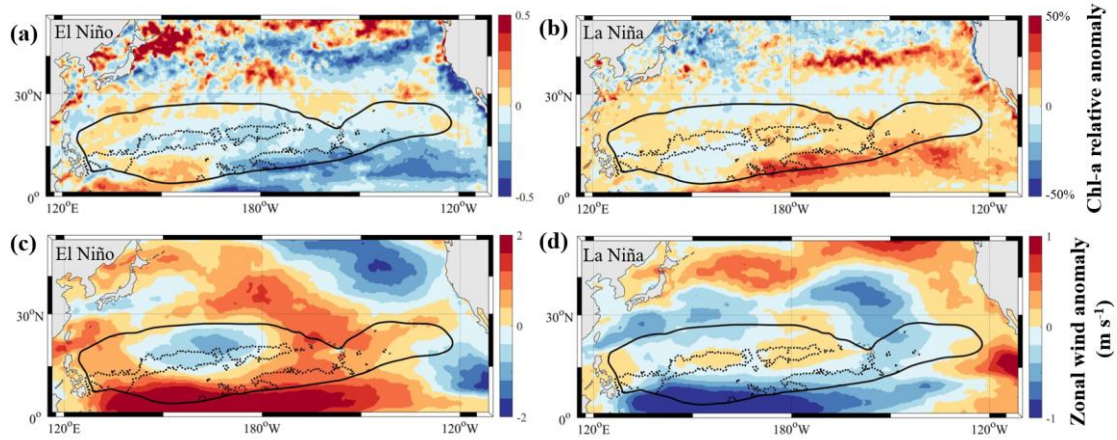
147

148

149

150

151



152

153 **Figure S8** (a-b) Chl-a concentration relative anomalies in May–July of El Niño years (a) and La
 154 Niña years (b) relative to climatological-mean May–July Chl concentration. (c-d) Zonal wind
 155 speed anomalies in April–September of El Niño years (c) and La Niña years (d). The solid black
 156 lines represent the NPOD geographical region, the dashed black lines represent the boundaries of
 157 NPOD_WHY and NPOD_SHY.

158

159

160

161

162

163

164

165

166

167

168

169

170

171

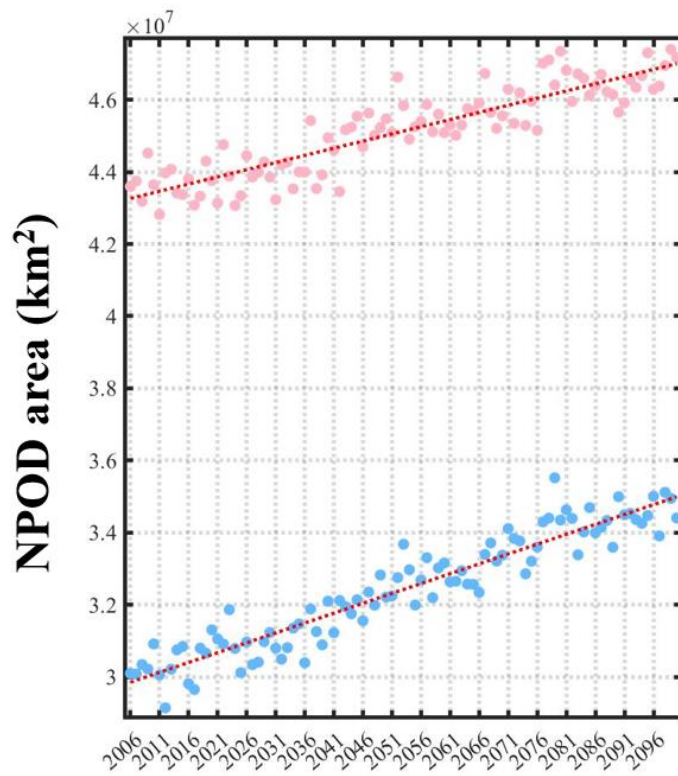
172

173

174

175

176



177

178 **Figure S9.** Time series of the NPOD-area seasonal maximum (pink) and minimum (blue) of
 179 NPOD area in 2006–2100 predicted by seven ESMS.

180

181

182

183

184

185

186

187

188

189

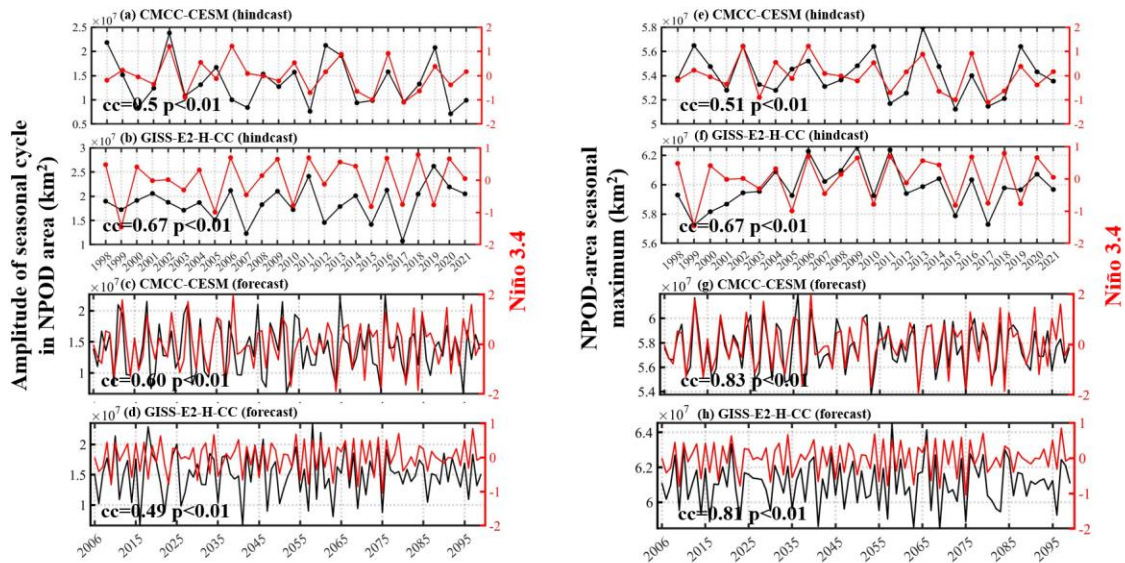
190

191

192

193

194



195

196 **Figure S10.** Time series of Niño 3.4 index are correlated with the NPOD-area seasonal amplitude
 197 in hindcast (a, b) and forecast (c, d) simulations by CMCC-CESM (a, c) and GISS-E2-H-CC (b,
 198 d) models. Time series of Niño 3.4 index are correlated with the NPOD-area seasonal maximum
 199 in hindcast (e, f) and forecast (g, h) simulations by CMCC-CESM (e, g) and GISS-E2-H-CC (f, h)
 200 models. 'cc' represents the correlation coefficient. In forecast simulations, the time series of
 201 NPOD area is detrended.

202

203

204

205

206

207

208

209

210

211

212

213

214

215

216

217

218 Table S1. Details of observational and reanalysis data

Variables	Sources/Products	Units	Temporal Resolution
Chl-a concentration	SeaWiFS & MODIS Level-3 Standard Mapped Images	mg m ⁻³	
SST	NOAA Optimum Interpolation (OI) SST, V2	°C	
Downward solar radiation and precipitation rate	European Centre for Medium-Range Weather Forecasts (ECWMF) ERA5 monthly averaged data on single levels	W m ⁻² , mm day ⁻¹	
Sea surface height relative to geoid	National Centers for Environmental Prediction (NCEP) Global Ocean Data Assimilation System (GODAS) provided by NOAA Physical Sciences Division	m	Monthly
Horizontal velocity components (u,v), temperature, salinity and mixed layer depth	Simple Ocean Data Assimilation version 3 (SODA3)	m s ⁻¹ , °C, m	
Nutrients (N+P) concentration	World Ocean Atlas (WOA) 2005	μmol L ⁻¹	
wind stress	ECMWF ORAS5	N m ⁻²	

219
220
221
222
223
224
225
226
227
228
229
230
231
232
233

234 Table S2. Overview of the output of Earth System Models in this study

Models	Institutions	Variables	Experiments
CMCC-CESM	Centro Euro-Mediterraneo per I Cambiamenti Climatici	SST, sea surface height, precipitation, solar radiation, wind stress, Chl-a	RCP 8.5
CNRM-CM5	National Center for Meteorological Research, Météo-France and CNRS laboratory		
GFDL-ESM2M	NOAA Geophysical Fluid Dynamics Laboratory		
GISS-E2-CC	NASA Goddard Institute for Space Studies (GISS)		
IPSL-CM5A-LR	Institut Pierre-Simon Laplace Climate Modelling Centre		
MIROC-ESM	Japan Agency for Marine-Earth Science and Technology, Atmosphere and Ocean Research Institute (The University of Tokyo), and National Institute for Environmental Studies		
MRI-CGCM3	Meteorological Research Institute		
CMCC-CESM	Centro Euro-Mediterraneo per I Cambiamenti Climatici		
CNRM-CM5	Centre National de Recherches Meteorologiques / Centre Europeen de Recherche et Formation Avancees en Calcul Scientifique		
IPSL-CM5A-LR	Institut Pierre-Simon Laplace		

235
 236
 237
 238
 239
 240
 241
 242
 243

244 Table S3. Performance of Elman Neural Network with different input variables

Input variables	SST, solar radiation	SST, wind stress curl	SST, sea surface height	SST, precipitation
Relative error of ENN (%)	7.45	8.38	8.98	9.02
Input variables	SST, solar radiation, wind stress curl	SST, precipitation, wind stress curl	SST, solar radiation, precipitation	SST, sea surface height, precipitation
Relative error of ENN (%)	7.06	7.89	7.99	10.35
Input variables	SST, sea surface height, solar radiation, wind stress curl	SST, sea surface height, precipitation, solar radiation	SST, precipitation, solar radiation, wind stress curl	
Relative error of ENN (%)	7.74	7.87	11.99	
Input variables	SST, solar radiation, precipitation, sea surface height, wind stress curl			
Relative error of ENN (%)	13.3			

245